Journal of Power Sources 201 (2012) 387–394

Contents lists available at SciVerse ScienceDirect

Journal of Power Sources

journal homepage: www.elsevier.com/locate/jpowsour

Improved the performance of dye-sensitized solar cells by incorporating mesoporous silica (SBA-15) materials in scattering layer

Chun-Chen Yang*, Yu Rong Zheng

Department of Chemical Engineering, MingChi University of Technology, New Taipei City 24301, Taiwan, ROC

ARTICLE INFO

Article history:
Received 19 October 2011
Accepted 31 October 2011
Available online 12 November 2011

Keywords:
Dye-sensitized solar cell
Scattering layer
Mesoporous silica
Molecular sieve
Incident photon to current efficiency

ABSTRACT

The surface-modified SBA-15 molecular sieve materials (denoted as m-SBA-15), which are incorporated into the scattering layer, are prepared on the P90 TiO_2 electrode to enhance the solar-conversion efficiency of the dye-sensitized solar cell (DSSC). The performance of the DSSC is also found to be further improved when the addition small amounts of TiO_2 nanorod (Tnr) in the photoelectrodes. It is found that the composite P90–Tnr TiO_2 photoelectrode with an m-SBA-15 scattering layer shows the highest amount of N3 dye adsorption (approximately 12.09×10^{-8} mol cm^{-2}); and also exhibits higher diffuse reflectance in the wavelength of 400–800 nm. The optimal electrochemical performance of the DSSC comprised of the composite P90–Tnr TiO_2 photoelectrode with the conversion efficiency (η) of approximately 6.94%, the short current density (J_{sc}) of 15.63 mA cm^{-2}, an open-circuit (V_{oc}) of 0.712 V, and a filler factor of 0.62 is obtained under illumination of 100 mW cm^{-2}. This study demonstrates that the addition small amounts of TiO_2 nanorods (Tnr) can enhance the electron transport properties and the incorporating large size SBA-15 silica into the scattering layer can greatly enhance the light absorption by the scattering effect while maintaining a higher dye adsorption.

1. Introduction

Dye-sensitized solar cell (DSSC) has become one of the most promising third-generation solar cells since O'Regan and Gratzel [1,2] reported a relatively high solar-energy conversion efficient of approximately 10–11% for the DSSC. The DSSCs have the advantages of low cost, easy mass production, simple fabrication equipment, and relatively high-energy conversion efficiency. A dye-sensitized solar cell consists of the following three main components: a dye-absorbed nanocrystalline TiO_2 film [3–16] on a transparent conductive oxide (TCO) substrate, referred to as the anode; an I^-/I_3^- redox couple in an organic solvent; and a platinized TCO substrate, the so-called the counter electrode (CE). The solar-energy conversion principle of the DSSC is based on the injection of electrons from the photo-excited state of a dye into the conduction band of TiO_2. The oxidized dye was then reduced by the iodide ions (I^-) in the electrolyte and the resulting tri-iodide ions (I_3^-) were reduced to iodide ions at the Pt counter electrode (that is, $I_3^- + 2e^- \rightarrow 3I^-$). The nanocrystalline TiO_2 shows a wide band gap of semiconductor material (that is, anatase 3.2 eV). Various TiO_2 morphologies have been proposed to fabricate the porous photoelectrodes, such as nanoparticles [3–6], nanotubes [7–10], nanowires [11], and nanofibers [12]. The commercially available P25 TiO_2 nanoparticles, which are used to prepare the thick TiO_2 films [13–16], have attracted significant attention, due to their high purity, availability, and relatively low cost.

The Pt counter electrode is used as a cathode, which plays an important role for the I_3^- reduction and electron transfer, where Pt serves as a catalyst [17–22]. The optimal performance of the counter electrode requires a low internal resistance and a low raw material cost. The highest performance material for the counter electrode is Pt, which exhibits an excellent electrochemical activity of the I_3^- reduction with a film thickness of 2–10 nm [5]. To achieve the desired catalytic performance for the I_3^- reduction, approximately 5–10 μg cm^{-2} of Pt was used.

The photoelectrode, using TiO_2 nanoparticles treated with $TiCl_4$, was prepared to reduce the dark current and enhance the conversion efficiency [23–26]. A number of authors [27–30] prepared the TiO_2 anode by a sol–gel method doping with metal ions [27,28] or metal oxides [29,30] to improve the power conversion efficiencies of the DSSCs. The electrochemical performance of the DSSCs was greatly enhanced by using large size TiO_2 nanoparticles in the range of 300–400 nm [31–33]. It is imperative to increase the light absorption by the scattering effect while maintaining a high surface area of the photoelectrodes for dye adsorption.

In this study, the porous TiO_2 photoelectrodes based on P90 TiO_2 nanoparticles (14 nm, 100 m^2 g^{-1}, Degussa) on FTO/glass were prepared by a doctor-blade method. The as-prepared TiO_2 electrodes

* Corresponding author. Tel.: +886 29089899; fax: +886 29041914.
E-mail address: ccyang@mail.mcut.edu.tw (C.-C. Yang).

0378-7753/$ – see front matter © 2011 Elsevier B.V. All rights reserved.
doi:10.1016/j.jpowsour.2011.10.111

were subsequently calcined at 450 °C for 30 min. The neat P90 TiO_2 electrode, the composite P90 TiO_2 electrode with m-SBA-15 scattering layer, and the composite P90–Tnr (1.5 wt.%) TiO_2 electrode with m-SBA-15 scattering layer obtained with thicknesses of 15.8, 18.4, and 18.6 μm, respectively. The Pt counter electrode was prepared by a pulse-deposition method on the FTO/glass substrate. The electrochemical performances of DSSCs comprised of various types. The P90 TiO_2 electrodes were examined by a linear scanning method and electrochemical impedance spectroscopy (EIS). UV–Vis spectroscopy, BET, and micro-Raman spectroscopy were also used to examine the properties of surface-modified SBA-15 powders. The effect of the SBA-15 scattering layer on the photoanodes in DSSCs for the solar harvesting efficiency was examined and discussed.

2. Experimental

2.1. Preparation of SBA-15 powders, TiO_2 nanorods, and P90 TiO_2 electrodes

The mesoporous SBA-15 (silica) powders were prepared by using a triblock copolymer ($EO_{20}PO_{70}EO_{20}$ or Pluronic 123, Aldrich)) and tetraethoxysilane (TEOS, Aldrich) as a silica source [34]. A 10 g of triblock copolymer was added to 300 mL of an aqueous solution of 2 M HCl and stirred at 50 °C for 2 h. Then, 20 g of TEOS was added gradually to the solution and the mixture was stirred at 50 °C for 2 h. The as-prepared gels were maintained at 110 °C for 24 h under static condition. The final products were filtered, washed with distilled water and dried at 25 °C for 24 h and then dried at 110 °C for another 24 h. The as-prepared samples were then calcined under N_2 atmosphere at 500 °C for 6 h. The as-prepared SBA-15 powders were further modified using titanium tetra-isopropoxide (TTIP, Aldrich). The appropriate amounts of SBA-15 powders were added to a 60 wt.% titanium isopropoxide solution under stirring condition for 30 min, and then washed by D.I. water and anhydrous alcohol several times. The modified SBA-15 powder is denoted as m-SBA-15 in this study. The m-SBA-15 powders were examined by SEM, BET, and micro-Raman spectroscopy. The TiO_2 nanorod (Tnr) powders were prepared by the hydrothermal process. The suitable amount of P90 TiO_2 powders dispersed in 10 M NaOH solution was transferred into a 600 mL Teflon-lined stainless steel autoclave, which was heated at 180 °C for 24 h. After the mixed solution cooled to room temperature, the precipitate powder was cleaned and dried at 60 °C for 10 h in a vacuum oven, followed by sintering process at 500–650 °C for 2 h under air atmosphere. The crystal structures of TiO_2 nano-rod samples were examined by using a Philips X'Pert X-ray diffractometer (XRD) with Cu Kα radiation of wavelength λ = 1.54056 Å for 2θ angles between 10° and 60°.

All of TiO_2 photoelectrodes were prepared by using lab-made TiO_2 paste on an F-doped tin oxide glass (FTO, 8 Ω sq.$^{-1}$, Aldrich), which is a doctor-blade method. The composition of the P90 TiO_2 paste was 4.0 g polyethylene glycol (PEG, M.W. 20,000, Fluka), 0.30 g Triton X-100 (Aldrich), 1.20 g acetylacetone (99%, Fisher Scientific), and 40.0 g TiO_2 nanocrystalline powders (P90, Degussa) in 100 g D.I water under continuous stirring condition for a minimum of 24 h. The as-coated TiO_2 photoelectrodes were sintered at 450 °C for 30 min. Various thicknesses of the P90 TiO_2 electrodes were obtained by a consecutive two-step process (that is, a coating step and a calcination step). Various thicknesses of the TiO_2 photoelectrodes were obtained, as followed: the P90 TiO_2 electrode of approximately 15.8 μm (denoted as the neat P90 TiO_2 electrode), the P90 TiO_2 electrode with a m-SBA-15 scattering layer of approximately 18.4 μm (denoted as the composite P90 TiO_2 electrode), and the 97.5 wt.% P90 TiO_2 nanoparticles + 2.5 wt.% TiO_2 nanorods composite electrode with a m-SBA-15 scattering layer of ca. 18.6 μm (denoted as the composite P90–Tnr TiO_2 electrode). Table 1 shows the compositions of the TiO_2 photoelectrodes containing various types of materials, the preparation conditions, and the thickness of the electrode for comparison. These TiO_2 anodes were then immersed in a solution of the dye ($RuL_2(NCS)_2{\cdot}2H_2O$, L = 2,2′-bipyridyl-4,4′-dicarboxylic acid, Ruthenium 535, N3 dye, Solaronix) with a concentration of 3×10^{-4} mol L^{-1} in dry ethanol for 24 h. The TiO_2 photoelectrodes with N3 dye were rinsed with anhydrous ethanol and dried again. In order to examine the loading amount of N3 dye in TiO_2 photoelectrodes, the dye was desorbed from the N3 adsorbed TiO_2 photoelectrodes into a NaOH aqueous solution (water/ethanol in 1:1, v/v, 1 M). The dye loading measurement was conducted by A UV-Vis spectrophotometer (JASCO V-570 spectrometer). The area of the photoanode was 0.25 cm^2.

2.2. Preparation of Pt counter electrodes

The Pt counter electrode was prepared from an aqueous solution containing 10 mM H_2PtCl_6, and 100 ppm PEG (M.W. 10,000) in a 0.50 M KCl solution; and a three-electrode cell, with the FTO/glass substrate, was used as the working electrode, the Pt wire was used as the counter electrode, and the SCE reference electrode was used. The FTO/glass conducting substrate with a dimension of 1 cm × 1 cm was cleaned by ethanol and D.I. water several times prior to the deposition. The galvanostatic pulse deposition of the Pt film on the FTO/glass was carried out at a constant current density of 5 mA cm^{-2} for t_{on} = 0.20 s, then zero current for t_{off} = 0.80 s. The duty cycle was defined as $D = t_{on}/(t_{on} + t_{off})$. The duty cycle ($D$) was maintained at 0.2. The total deposition charge was 300 mC; the thickness of the pulse-plated Pt films was controlled at approximately 5 nm.

2.3. Characterization of the TiO_2 photoelectrodes

The P90 TiO_2 photoelectrodes without and with the m-SBA-15 scattering layer were characterized by a scanning electron microscope (SEM, a Hitachi S-2600H, Japan) to examine their surface morphology and the coating thickness of the porous TiO_2 films. The absorbance and diffuse reflectance of the P90 TiO_2 photoelectrodes were measured by using a UV-Vis spectrophotometer (Jasco 470).

2.4. DSSC assembly and measurements

The DSSCs with an active area of 0.25 cm^2 were assembled by using the N3 sensitizing P90 TiO_2 photoelectrodes and the Pt counter electrodes. All cells were sealed by using a thickness of 30 μm Surlyn (Du Pont). The Surlyn polymer film acted as a spacer and the cell gap was fixed at approximately 30 μm. The two holes were made on the counter electrode and the cell was heated at 100 °C for 10 s on a hot plate until the Surlyn film had completely melted. The electrolyte was then injected into the spacer between the electrodes through these two holes. Finally, these two holes were completely resealed by the Surlyn film and glass. The electrolyte was composed of 6 M dimethylpropylimidazolium iodide (DMPII), 0.1 M lithium iodide (LiI), 0.05 M iodine (I_2), and 0.50 M 4-tert-butylpyridine (TBP) in CH_3CN. All electrochemical measurements for DSSCs were carried out in a two-electrode system. The photovoltaic characteristics of DSSCs were measured by using a Solar Simulator (300W Oriel), under 1.5 AM (100 mW cm^{-2}) irradiation. The I–V and AC spectra of DSSCs based on the P90 TiO_2 anodes, with and without the scattering layer, were measured by an Autolab PGSTAT-30 electrochemical system with GPES 4.8 package software (Eco Chemie, The Netherlands) at room temperature. The detailed construction and measurement of the DSSC have been published [3–6].

Table 1
The compositions of the TiO_2 photoelectrodes containing with various types materials.

Samples	Types				
	Materials and compositions			Processing condition	Thickness
	First layer (as porous layer)	Second layer (as porous layer)	Third layer (as scattering layer)		
Neat P90 TiO_2 electrode	P90	P90	–	Sintered at 450 °C, 30 min, two times	15.8 μm
Composite P90 TiO_2 electrode	P90	P90	m-SBA-15:P90 = 1:1	Sintered at 450 °C, 30 min, three times	18.4 μm
Composite P90–Tnr TiO_2 electrode	P90:Tnr = 0.975:0.025[a]	P90:Tnr = 0.975:0.025	m-SBA-15:P90 = 1:1[a]	Sintered at 450 °C, 30 min, three times	18.6 μm

[a] All in weight ratio.

3. Results and discussion

3.1. Morphology analysis

Fig. 1(a) and (b) shows the SEM photographs of the as-prepared SBA-15 and m-SBA-15 powders, respectively, in which the surface was deposited with TiO_2 nanoparticles. It was found that those SBA-15 powders or aggregates reveal a long tube shape. The length of the SBA-15 aggregates was approximately 1–10 μm. The SBA-15 powder is a mesoporous material with a high specific surface area, large dimension open channels (5–50 nm), and excellent thermal and chemical stability [34]. As seen in Fig. 1(b), the surface morphology of m-SBA-15 powders was not altered; and the HR-TEM result shows the SBA-15 powder with a hexagonal structure (result not shown here).

The N_2 adsorption–desorption isotherm (or BET isotherm) at 77 K for the as-prepared SBA-15 and the m-SBA-15 powders is shown in Fig. 2(a). The N_2 adsorption isotherm of the SBA-15 materials is a typical reversible type IV adsorption isotherm, which has a characteristic of a mesoporous material. The BET results also indicated that the specific surface area (S.A.) of SBA-15 and m-SBA-15 powders was 571 $m^2\ g^{-1}$ and 184 $m^2\ g^{-1}$, respectively. The pore side distribution was in the range of 2–200 nm and centered at approximately 8 nm, as shown in Fig. 2(b). As expected, the surface area of the m-SBA-15 materials markedly decreased; which may be due to the TiO_2 nanoparticles coated on the top surface of SBA-15 powders. Those TiO_2 nanoparticles may block some surface area of SBA-15 powders. The TiO_2 nanoparticles anchored on SBA-15 powders can facilitate N3 dye adsorption and significantly enhance the light scattering and the electron charge transport rate [30].

Fig. 3 shows the micro-Raman spectra of m-SBA-15 powders and commercial P90 TiO_2 nanoparticles (Degussa). Generally, the composition of commercially available P90 powders is approximately 90 wt.% anatase (major) phase and 10 wt.% rutile (minor) phase. It

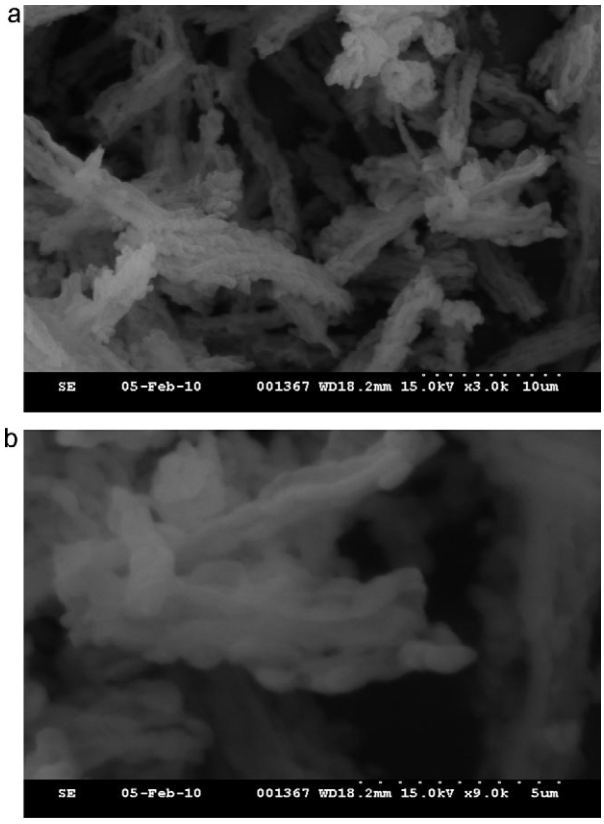

Fig. 1. SEM images for: (a) as-prepared SBA-15 powders; (b) m-SBA-15 powders.

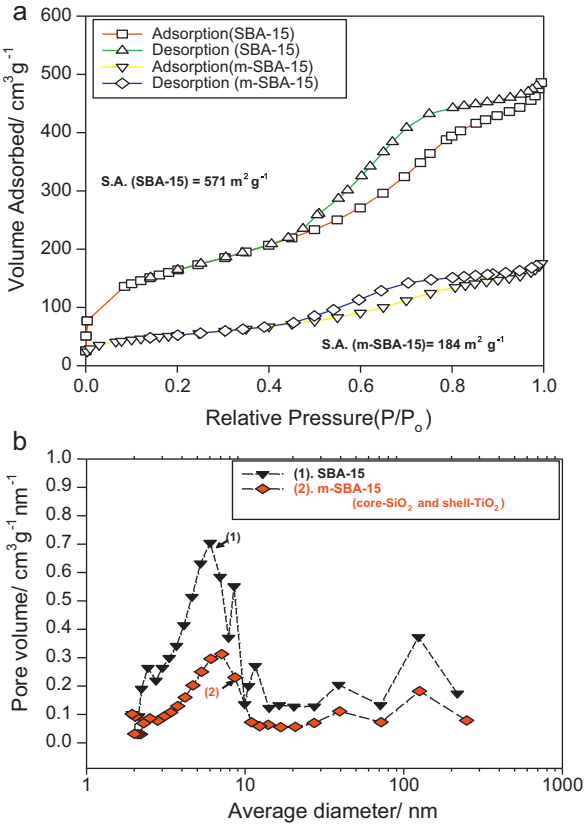

Fig. 2. (a) Nitrogen adsorption isotherm pattern; (b) the pore size distribution of the as-prepared and modified SBA-15 powders.

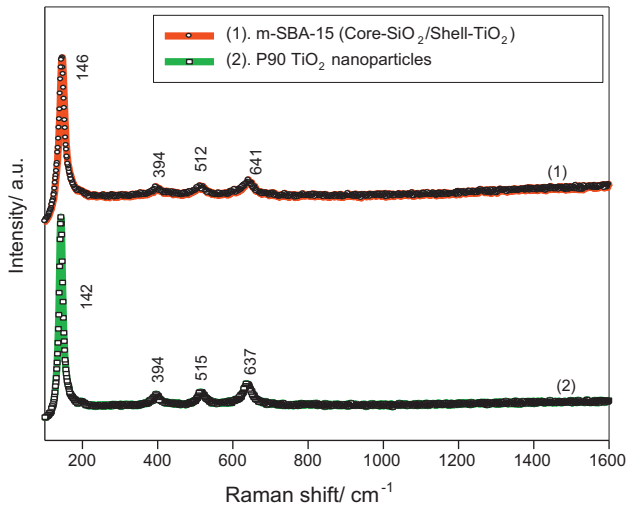

Fig. 3. Micro-Raman spectra of m-SBA-15 powders and P90 TiO_2 nanoparticles.

was found that there are four major peaks for TiO_2 samples, and that these scattering bands were located at 142–146, 394–395, 512–515, and 635–641 cm^{-1}, corresponding to the characteristic peaks of anatase TiO_2. The 144 and 395 cm^{-1} bands are due to O–Ti–O bond bending; the 512 and 635 cm^{-1} bands are due to Ti–O bond stretching. The micro-Raman spectrum of the m-SBA-15 powders is the same as pure anatase TiO_2 powders, indicating that anatase TiO_2 nanoparticles are anchored on the top surface of the m-SBA-15 powders.

Fig. 4 shows the XRD patterns of the as-prepared and sintered TiO_2 nanorod (Tnr) samples (at temperatures of 500–650 °C) and P90 TiO_2 powders for comparison. It is observed that the degree of crystallinity of TiO_2 nanorod powders increases when the sintering temperature is higher than 600 °C. Importantly, the XRD results also indicate that P90 TiO_2 powders show the major anatase and minor rutile phases. In contrast, our as-prepared TiO_2 nanorod samples

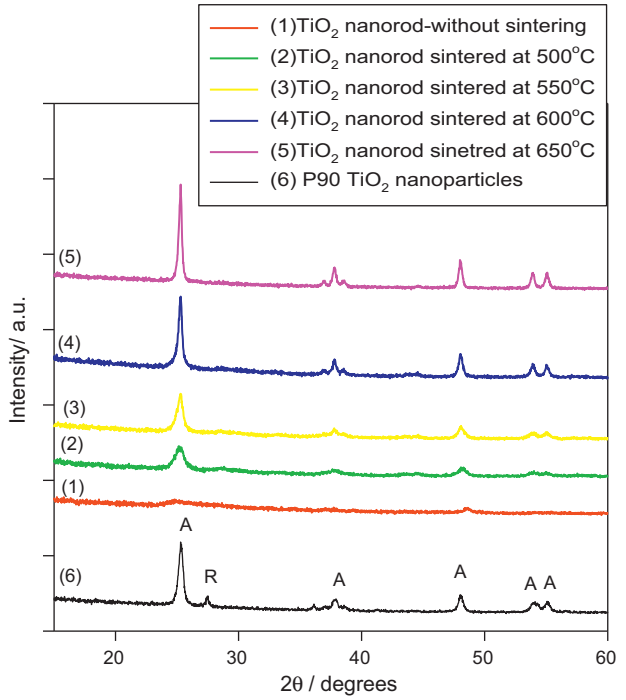

Fig. 4. XRD patterns of TiO_2 nanorods (Tnr) sintered at different temperatures.

show a pure anatase phase. Therefore, all TiO_2 nanorod samples used in the composite P90–Tnr electrode were sintered at 600 °C.

Fig. 5(a)–(d) shows the top- and cross-section views of SEM photographs for the composite P90 TiO_2 electrode comprised of the m-SBA-15 scattering layer. As seen in Fig. 5(a)–(d), the composite P90 TiO_2 electrode shows a uniform and homogenous surface; however, there are still a number of micro-crevices present, which is due to the fast evaporation of the deionized water from the top surface of the coated TiO_2 electrode. However, the size of microcracks was significantly reduced when the scattering layer was applied. The composition of the porous layer or underlayer for the composite P90–Tnr TiO_2 electrode was 97.5 wt.% for P90 TiO_2 powders and 1.5 wt.% for TiO_2 nanorod powders. It was found that when the TiO_2 nanorods were added into the photoelectrodes, the electron transport rate can be improved. By contrast, the composition of the scattering layer was 50 wt.% for P90 and 50 wt.% for m-SBA-15 powders. The dispersing ability and uniformity of the scattering layer paste were significantly improved when the scattering paste contained P90 nanoparticles. It was discovered that the scattering layer paste that only contained m-SBA-15 was difficult to disperse and peel off. The thickness of the composite P90 TiO_2 electrode was approximately 18.6 μm; and was estimated from the cross-section view of the SEM photograph, as shown in Fig. 5(d).

3.2. Optical property analysis of the TiO_2 photoelectrodes

Fig. 6(a) and (b) displays the UV–Vis absorbance of the neat P90 TiO_2 electrode, the composite P90 TiO_2 electrode with a m-SBA-15 scattering layer, and the composite P90–Tnr TiO_2 electrode with a m-SBA-15 scattering layer without and with N3 dye, respectively. The absorbance intensity of the composite P90 or P90–Tnr TiO_2 electrode was significantly increased when the m-SBA-15 scattering layer was used on the photoelectrodes. However, the absorbance intensity of both the composite P90 TiO_2 electrode and the composite P90–Tnr TiO_2 electrode is comparable. This is due to the same chemical composition for both photoelectrodes; and both contain the m-SBA-15 scattering layer.

Fig. 6(c) and (d) shows the UV–Vis reflectance spectra for the neat P90 TiO_2 electrode, the composite P90 TiO_2 electrode with an m-SBA-15 scattering layer, and the composite P90–Tnr TiO_2 electrode with an m-SBA-15 scattering layer without and with N3 dye, respectively. As seen in Fig. 6(c), the reflectance value of the neat P90 electrode (without a scattering layer) is lower than those of the composite P90 and P90–Tnr TiO_2 electrodes, and is due to the light scattering effect by the large size SBA-15 powders. The neat P90 TiO_2 electrode without N3 dye shows diffuse reflectance of 14–20% in the wavelength of 600–800 nm. However, the composite P90 TiO_2 electrode without N3 dye shows the highest diffuse reflectance of 25–34% in the wavelength of 600–800 nm. The reflectance value of the composite P90–Tnr TiO_2 electrode is only slightly lower than that of the composite P90 TiO_2 electrode. By contrast, the diffuse reflectance value of composite P90 or P90–Tnr TiO_2 electrode is significantly higher; and is due to the addition of the scattering layer in the photoelectrode. The excellent light reflectance properties for the composite P90 TiO_2 electrode with mesoporous structure m-SBA-15 materials were demonstrated.

The amounts of N3 dye absorbed in the TiO_2 photoelectrodes markedly affect the electrochemical performance of the DSSCs. As a result, it was found that the amounts of N3 dye absorbed in neat P90 TiO_2 electrode, the composite P90 TiO_2 electrode, and the composite P90–Tnr TiO_2 electrode are 6.92×10^{-8}, 8.98×10^{-8}, and 12.09×10^{-8} mol cm^{-2}, respectively. It was found that the composite P90–Tnr TiO_2 photoelectrode with a m-SBA-15 scattering layer showed the highest amount of N3 dye adsorption, i.e., 12.09×10^{-8} mol cm^{-2}. It was demonstrated clearly that the large size particles of m-SBA-15 materials used on the scattering layer

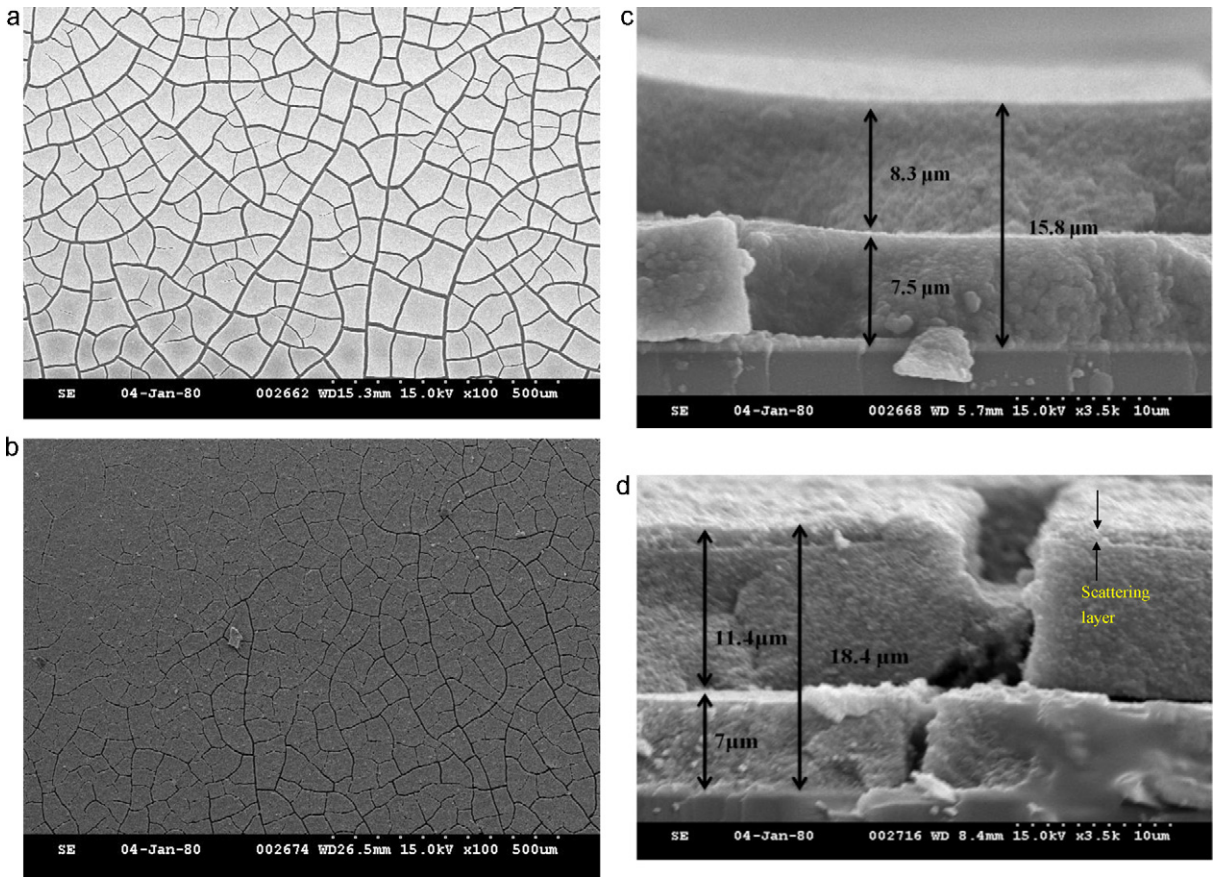

Fig. 5. SEM images of TiO_2 electrodes: (a and b) top views of the neat P90 and the composite P90 TiO_2 electrodes; (c and d) cross-section views of the neat P90 film and the composite P90 TiO_2 electrodes.

did not decrease the amount of N3 dye absorption in the photoelectrodes.

3.3. The photocurrent–voltage (I–V) property measurements

The photocurrent–voltage (*I–V*) characteristics of DSSCs comprised of varied types of the P90 TiO_2 electrodes and measured under AM 1.5, 100 mW cm^{-2} illuminations, and are shown in Fig. 7. The photovoltaic parameters of the cells can be obtained from the analysis of the *I–V* curves, including: (1) the open circuit voltage, V_{oc}; (2) the short circuit photocurrent density, J_{sc}; (3) the fill factor, FF; and (4) the cell's overall energy conversion efficiency of the cell, η. The cell's fill factor (FF) can be estimated by Eq. (1):

$$\mathrm{FF} = \frac{V_{max}J_{max}}{V_{oc}J_{sc}} \quad (1)$$

where V_{max} and J_{max} are the voltage and the current density, respectively, for the maximum power output. Taking into account the FF parameter, the energy conversion efficiency can be estimated from Eq. (2), as follows:

$$\eta\ (\%) = \frac{V_{oc}J_{sc}\,\mathrm{FF}}{P_{in}} \times 100 \quad (2)$$

The detailed results of the photovoltaic parameters of DSSCs are listed in Table 2. As a result, when the varied types of the P90 TiO_2 electrodes, including the neat P90 electrode, the composite P90 TiO_2 electrode, and the composite P90–Tnr TiO_2 electrode, were used on the DSSC, the values of V_{oc} were 0.671, 0.709, and 0.712 V, respectively. In addition, the J_{sc} was significantly increased, from 11.13 to 15.63 mA cm^{-2}. The FF remained stable at a range of 0.62–0.68. The FF mainly relates to the series resistance or the ohmic loss of the cell [31–33]. The energy conversion efficiency (η) was enhanced when the thicknesses of the TiO_2 photoelectrode were increased.

In particular, the DSSC with the composite P90–Tnr TiO_2 electrode, consisting of a porous Tnr TiO_2 underlayer and an m-SBA-15 scattering overlayer, shows the conversion efficiency of 6.94%. It was found that the amounts of adsorbed N3 dye of the composite P90 TiO_2 electrode were approximately $(6.92–8.98) \times 10^{-8}$ mol cm^{-2}. The higher thickness of the composite P90–Tnr TiO_2 electrode results in higher amounts of absorbed dye.

3.4. EIS characterizations

The AC impedance spectroscopy is a powerful tool to examine the influence of various resistive elements on the DSSC. Fig. 8 shows the Nyquist plot of the DSSC comprised of the P90 TiO_2 electrodes with and without the m-SBA-15 scattering layer under 100 mW cm^{-2} illuminations with an open-circuit voltage. The typical Nyquist plot contains three semicircles, which are assigned in the order of decreasing frequency to the electrochemical reaction at the Pt counter electrode (R_{ct1}), the charge transfer at the TiO_2/dye/electrolyte (R_{ct2}) and the Warburg diffusion process of I^-/I_3^- ions (Z_w) [30–33]. All of the AC impedance parameters, such as R_b, R_{ct1}, R_{ct2} and τ_e, are listed in Table 3. The values of series resistances (R_b) are 17.31 and 15.32 Ω for DSSCs based on the neat P90 TiO_2 electrodes without the scattering layer and the composite P90 TiO_2 electrode with the scattering layer, respectively. On the other hand, the R_{ct1} values for the charge transfer resistance at the Pt counter electrode were at a range of 2.07–3.75 Ω, and showed

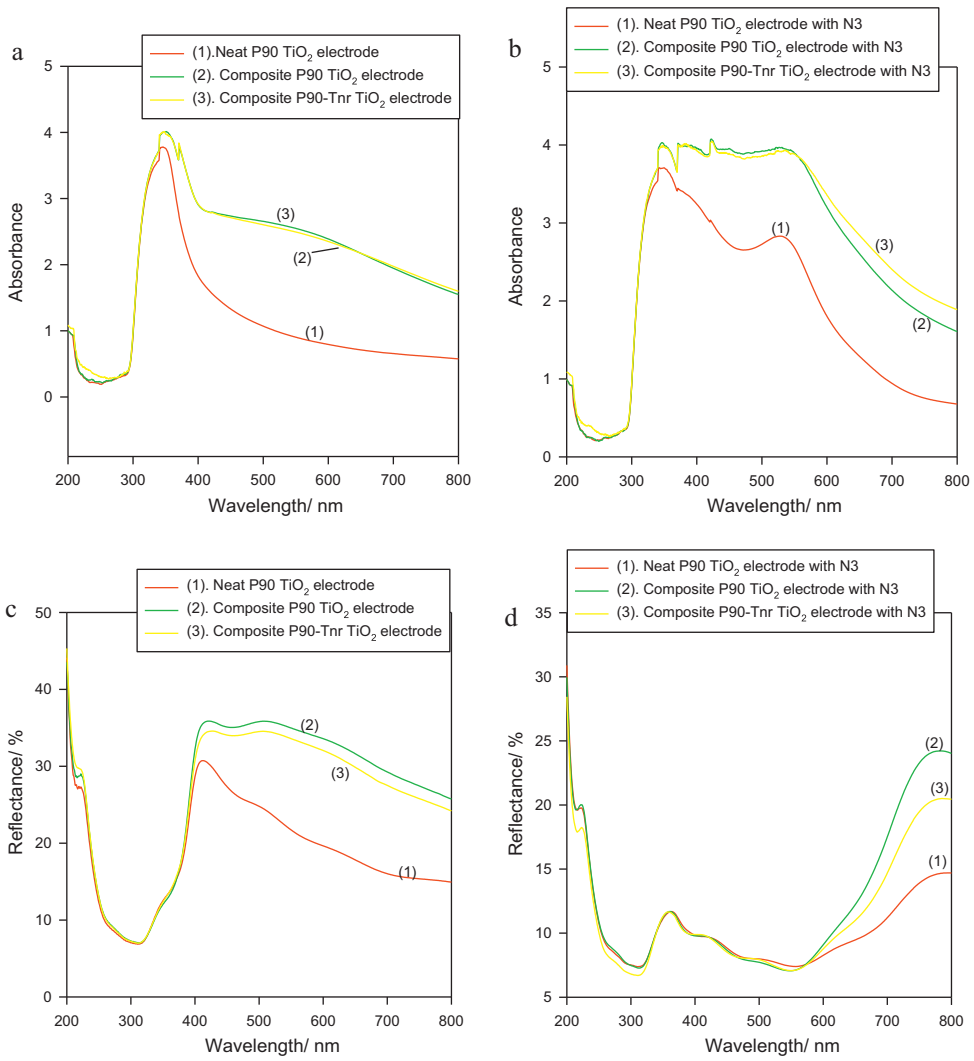

Fig. 6. The absorbance spectra for the TiO_2 photoanodes: (a and b) without and with N3 dye, respectively; the reflectance spectra for the TiO_2 photoanodes: (c and d) without and with N3 dye, respectively.

Table 2
The photovoltaic parameters of the DSSCs with various types P90 TiO_2 photoelectrodes.

Anodes	Parameters					
	V_{oc} (V)	J_{sc} (mA cm^{-2})	V_{max} (V)	J_{max} (mA cm^{-2})	FF	((%)
Neat P90 TiO_2 electrode	0.671	11.13	0.487	10.38	0.68	5.05
Composite P90 TiO_2 electrode	0.709	12.94	0.523	11.85	0.62	6.20
Composite P90–Tnr TiO_2 electrode	0.712	15.63	0.487	14.25	0.62	6.94

minimal variations. The R_{ct2} value was varied at 14.35–18.90 Ω. Furthermore, it was found that the electron lifetime (τ_e) value was increased from 9.37 to 17.85 ms when the scattering layer was used on the TiO_2 photoelectrode. It is well-known that one dimensional titania nanorods (Tnr TiO_2) can provide a direct electrical pathway for photogenerated electron to increase the electron transport rate [30–33]. The DSSC composed of the composite P90–Tnr TiO_2 electrode with the m-SBA-15 + P90 (1:1) scattering layer exhibits the longest electron life time of 17.85 ms. In general, the higher the electron lifetime, the more efficient is the performance of the DSSCs [32].

Table 3
AC impedance analysis results of the DSSCs with various types of the photoelectrodes.

Anodes	Parameters			
	R_b (Ω)	R_{ct1} (Ω)	R_{ct2} (Ω)	τ_e (ms)
Neat P90 TiO_2 electrode	17.31	2.07	18.90	9.37
Composite P90 TiO_2 electrode	15.32	2.56	15.07	15.33
Composite P90–Tnr TiO_2 electrode	13.73	3.75	14.35	17.85

The DSSC which is comprised of the composite P90 TiO_2 electrode with the mesoporous scattering layer (approximately 3 μm) can achieve the higher energy efficiency (6.29%), as compared with the neat P90 TiO_2 photoelectrode without a scattering layer (5.05%). It is observed that the TiO_2 photoelectrode, which is comprised of the non-porous scattering layer, tends to decrease the amount of dye adsorption on the TiO_2 photoelectrodes; and will result in the lower J_{sc} and η values. When the TiO_2 photoelectrode comprised of the mesoporous SBA-15 scattering layer tends to increase the

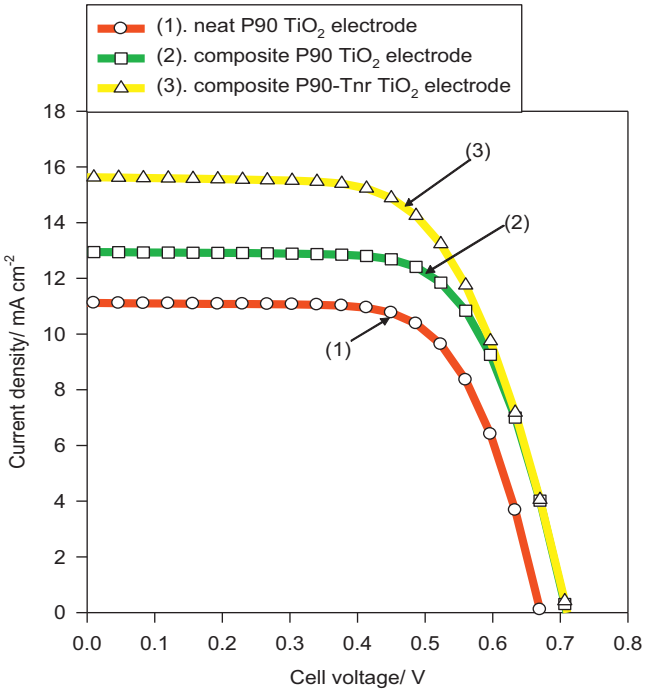

Fig. 7. The *I–V* curves of the DSSCs with varied types of P90 TiO_2 photoelectrodes.

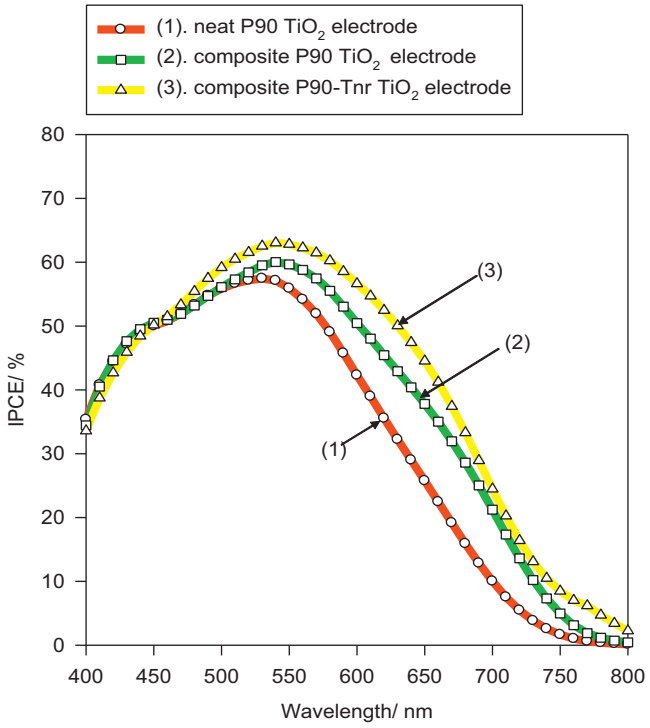

Fig. 9. The IPCE curves of the DSSCs with varied types of P90 TiO_2 electrodes.

amount of dye adsorption, the photo-light conversion efficiency can be significantly improved. It is necessary to increase the light absorption by a scattering layer while maintaining a higher internal surface area of the photoanodes for efficient dye adsorption. The m-SBA-15 powders with a specific area of 184 $m^2\ g^{-1}$ and the aggregate size of 1–10 μm [34] play a vital role in improving the light harvest efficiency and cell performance.

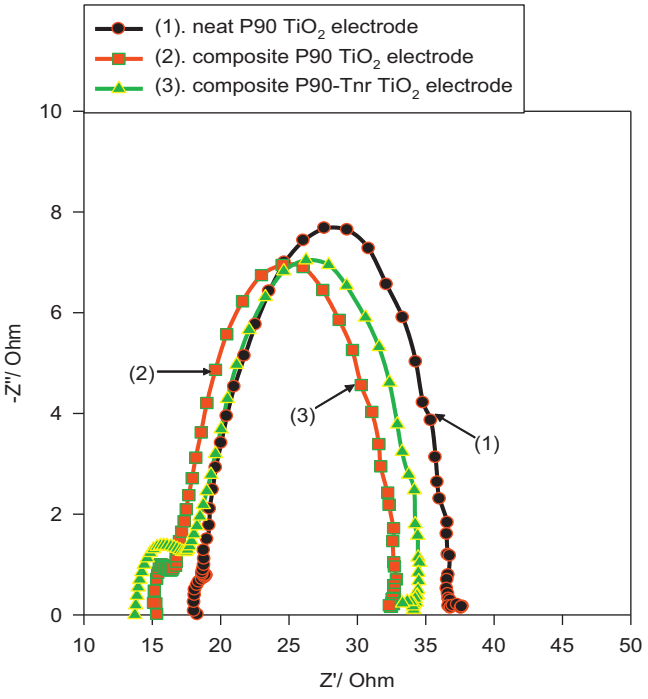

Fig. 8. The AC impedance spectra of the DSSCs with varied types of P90 TiO_2 photoelectrodes.

3.5. IPCE analysis

Fig. 9 shows the incident photon to current efficiency (IPCE) results for the DSSCs comprised of the P90 TiO_2 electrodes with and without the m-SBA-15 scattering layer, and the composite P90–Tnr TiO_2 electrode. The maximum IPCE values of DSSCs occurred at approximately 540 nm, corresponding to the N3 dye adsorption peak. A noticeable difference on the three types of the samples was observed. The DSSC comprised of the m-SBA-15 scattering layer exhibit a higher IPCE value; which is due to the scattering layer effect on the electrode.

Accordingly, the DSSC with the composite P90–Tnr TiO_2 electrode (with the scattering SBA-15 layer) shows significantly higher IPCE value in the wavelength of 600–800 nm. The DSSC with a higher IPCE value also exhibited superior to electrochemical performance; and has been demonstrated as an ideal candidate for a future DSSC application.

4. Conclusions

The neat TiO_2 electrode and the composite P90 TiO_2 or P90–Tnr TiO_2 electrode comprised of the m-SBA-15 scattering layer were obtained by a doctor-blade method in this study for the first time. All of the P90 TiO_2 electrodes were subsequently carried out by a calcinating step at 450 °C. The dye-sensitized solar cells (DSSCs) were assembled with the P90 TiO_2 electrodes and the pulse-plated Pt counter electrodes. The DSSC which comprised of the composite P90–Tnr TiO_2 electrode with a m-SBA-15 scattering layer achieved the highest conversion efficiency of approximately 6.94% with J_{sc} of 15.63 mA cm^{-2}, with an open-circuit (V_{oc}) of 0.712 V and a filler factor of 0.62 under illumination of 100 mW cm^{-2}. The results indicated that the dye-sensitized solar cells (DSSCs) with those composite P90–Tnr TiO_2 electrodes displayed excellent energy efficiency and electrochemical performance. The composite P90–Tnr TiO_2 photoelectrode has been demonstrated as an ideal candidate for future DSSC applications.

Acknowledgement

The financial support from the National Science Council, Taiwan (Project No. NSC-96-2221-E131-009-MY2) is gratefully acknowledged.

References

[1] B. O'Regan, M. Gratzel, Nature 353 (1991) 737.
[2] M. Gratzel, Nature 414 (2001) 338.
[3] A. Hauch, A. Georg, Electrochim. Acta 46 (2001) 3457.
[4] L.M. Peter, N.W. Duffy, R.L. Wang, K.G.U. Wijayantha, J. Electroanal. Chem. 524–525 (2002) 127.
[5] X. Fang, T. Ma, G. Guan, M. Akiyama, T. Kida, E. Abe, J. Electroanal. Chem. 570 (2004) 257.
[6] X. Fang, T. Ma, G. Guan, M. Akiyama, E. Abe, J. Photochem. Photobiol. A 164 (2004) 179.
[7] T. Ma, X. Fang, M. Akiyama, K. Inoue, H. Noma, E. Abe, J. Electroanal. Chem. 574 (2004) 77.
[8] P. Li, J. Wu, J. Lin, M. Huang, Electrochim. Acta 53 (2008) 4161.
[9] C.H. Yoon, R. Vittal, J. Lee, W.S. Chae, K.J. Kim, Electrochim. Acta 53 (2008) 2890.
[10] G. Tsekouras, A.J. Mozer, G.G. Wallace, J. Electrochem. Soc. 155 (7) (2008) K124.
[11] K. Imoto, K. Takahashi, T. Yamaguchi, T. Komura, J.I. Nakamura, K. Murata, Solar Energy Mater. Solar Cells 79 (2003) 459.
[12] F. Cai, J. Liang, Z. Tao, J. Chen, R. Xu, J. Power Sources 177 (2008) 631.
[13] W.J. Lee, E. Ramasamy, D.Y. Lee, J.S. Song, Solar Energy Mater. Solar Cells 92 (2008) 814.
[14] Z. Huang, X. Liu, K. Li, D. Li, Y. Luo, H. Li, W. Song, L. Chen, Q. Meng, Electrochem. Commun. 9 (2007) 596.
[15] W.J. Lee, E. Ramasamy, D.Y. Lee, J.S. Song, J. Photochem. Photobiol. A 194 (2008) 27.
[16] B.K. Koo, D.Y. lee, H.J. Kim, W.J. Lee, J.S. Song, H.J. Kim, J. Electroceram. 17 (2006) 79.
[17] G. Khelashvili, S. Behrens, A. Hinsch, W. Habicht, D. Schild, A. Eichhofer, R. Sastrawan, K. Skupien, E. Dinjus, H. Bonnemann, Thin Solid Films 515 (2007) 4074.
[18] S.S. Kim, K.W. Park, J.H. Yum, Y.E. Sung, J. Photochem. Photobiol. A 189 (2007) 301.
[19] T. Hino, Y. Ogawa, N. Kuramoto, Carbon 44 (2006) 880.
[20] M. Biancardo, K. West, F.C. Krebs, J. Photochem. Photobiol. A 187 (2007) 395.
[21] R. Zhang, J. Pan, E.P. Brigg, M. Thrash, L.L. Kerr, Solar Energy Mater. Solar Cells 92 (2008) 425.
[22] T. Stergiopoulos, M.C. Bernard, A.H.L. Giff, P. Falaras, Coord. Chem. Rev. 248 (2004) 1407.
[23] L.Y. Zeng, S.Y. Dai, K.J. Wang, X. Pan, C.W. Shi, Li. Guo, Chin. Phys. Lett. 21 (2004) 1835.
[24] S. Ito, P. Liska, P. Comte, R. Charvet, P. Péchy, U. Bach, S.M. Lukas, S.M. Zakeeruddin, A. Kay, M.K. Nazeeruddin, M. Grätzel, Chem. Commun. 34 (2005) 4351.
[25] Y. Ohsaki, N. Masaki, T. Kitamura, Y. Wada, T. Okamoto, T. Sekino, K. Niihara, S. Yanagida, Phys. Chem. Chem. Phys. 7 (2005) 4157.
[26] H. Yu, S. Zhang, H. Zhao, G. Will, P. Liu, Electrochim. Acta 54 (2009) 1319.
[27] Y. Wang, Y. Hao, H. Cheng, J. Ma, B. Xu, W. Li, A. Cai, J. Mater. Sci. 34 (1999) 2773.
[28] K.H. Ko, Y.C. Lee, Y.J. Jung, J. Colloid Interface Sci. 283 (2005) 482.
[29] A. Kitiyanan, S. Yoshikawa, Mater. Lett. 59 (2005) 4038.
[30] T.V. Nguyen, H.C. Lee, M. Alam Khan, O.B. Yang, Solar Energy 81 (2007) 529.
[31] J. Ferber, J. Luther, Mater. Solar Cells 54 (1998) 265.
[32] J.K. Lee, B.H. Jeong, S.I. Jang, Y.S. Yeo, S.H. Park, J.U. Kim, Y.G. Kim, Y.W. Jang, M.R. Kim, J. Mater. Sci. 20 (2009) S446.
[33] K. Shin, Y. Jun, J.H. Moon, J.H. Park, Appl. Mater. Interface 2 (2010) 288.
[34] D.Y. Zhao, J.L. Feng, Q.S. Huo, N. Melosh, G.H. Fredrickson, B.F. Chmelka, G.D. Stucky, Science 279 (1998) 548.